Solution-Processed Low Threshold Vertical Cavity Surface Emitting Lasers from All-Inorganic Perovskite Nanocrystals

Wang, Yue; Li, Xiaoming; Nalla, Venkatram; Zeng, Haibo; Sun, Handong

2017

Wang, Y., Li, X., Nalla, V., Zeng, H., & Sun, H. (2017). Solution-Processed Low Threshold Vertical Cavity Surface Emitting Lasers from All-Inorganic Perovskite Nanocrystals. Advanced Functional Materials, 27(13), 1605088-.

https://hdl.handle.net/10356/83307

https://doi.org/10.1002/adfm.201605088

Solution-processed low threshold vertical cavity surface emitting lasers from all-inorganic perovskite nanocrystals

Yue Wang[1], Xiaoming Li[2,3], Venkatram Nalla[4], Haibo zeng[2*], Handong Sun[1,4*]

[1]Division of Physics and Applied Physics, School of Physical and Mathematical Sciences, Nanyang Technological University, Singapore 637371, Singapore

[2]Institute of Optoelectronics & Nanomaterials, College of Materials Science and Engineering Nanjing University of Science and Technology Nanjing, 210094, China

[3]State Key Laboratory of Mechanics and Control of Mechanical Structures, College of Materials Science and Engineering, Nanjing University of Aeronautics and Astronautics, Nanjing 210085, China

[4]Centre for Disruptive Photonic Technologies (CDPT), Nanyang Technological University, Singapore 637371, Singapore

* Authors to whom correspondence should be addressed, electronic email: hdsun@ntu.edu.sg, zeng.haibo@njust.edu.cn.

Abstract: Recently, all-inorganic cesium lead halide perovskite nanocrystals (IPNCs) ($CsPbX_3$, X = Cl, Br, I) were discovered to possess superior optical gain properties appealing for solution-processed cost-effective lasers. Yet, the potential of such materials has not been exploited for practical laser devices, rendering the prospect as laser media elusive. Herein, we realized for the first time the challenging but practically desirable vertical cavity surface emitting lasers (VCSELs) based on the $CsPbX_3$ IPNCs, featuring low threshold (9 μJ/cm^2), unidirectional output (beam divergence of ~3.6º) and favorable stability. The lasing wavelength can be tuned across red, green and blue region maintaining comparable thresholds, which is promising in developing single source-pumped full-color visible lasers. It is fully demonstrated that the characteristics of the

VCSELs can be versatilely engineered by independent adjustment of the cavity and solution processable nanocrystals. Our results represent a significant leap towards practical laser sources leveraging on the advantageous $CsPbX_3$ IPNCs.

Solution-processed gain materials are being pursued with the promise to revolutionize the vacuum-based epitaxial semiconductor lasers aiming at developing low-cost yet high-performance laser source[1]. Colloidal quantum dot (CQD) has been recognized as the ideal candidate due to the tunable emission color, enhanced optical properties and facile solution processiblity[2-4]. Ever since the first demonstration of stimulated emission from metal-chalcogenide CQDs in 2000[2], significant progress has been made in improving the lasing performance[5, 6]. However, the relatively low absorption cross-section and the high optical loss due to carrier trapping and Auger recombination (AR) still hinder the advance of CQD-lasers, especially in the short visible spectral range of blue and green[7, 8].

In the past years, the organic–inorganic halide perovskites, which have demonstrated impressive photovoltaic performance[9, 10], were also discovered to be potential optical gain media[11, 12]. However, the commercial aspirations may be stifled by the inherent instability of these hybrid perovskites[11, 12]. More recently, the newly engineered all-inorganic cesium lead halide ($CsPbX_3$ (X=Cl, Br and I)) perovskite nanocrystals are resurging as a superior optical gain material because of the large optical absorption cross-section, large exciton binding energy, high photoluminescence (PL) quantum yield and relatively low AR loss[13, 14]. Importantly, these all-inorganic perovskite nanocrystals (IPNCs) show much enhanced endurance to ambient environment than the organic-inorganic analogues[13, 15, 16]. Compared to traditional metal-chalcogenide CQDs, these $CsPbX_3$ IPNCs feature in narrow emission spectra, simple fabrication process, ease of color tunability by anion exchange, superior optical gain properties and so on[17-20]. As a result, these new emerging $CsPbX_3$ IPNCs can be envisioned as the promising solution towards inexpensive laser sources in the future.

So far, lasers based on single $CsPbX_3$ nanowire have been reported[21, 22]. Regarding lasers made from the ensemble of inorganic perovskite nanocrystals, only whispering gallery mode and random lasers which are among the easiest configurations for lasers have been demonstrated as a proof of concept[13, 14]. However, both of these laser types lack directionality, one of the most important advantages of a laser. Moreover, all of the above lasing demonstrations fall in multi-mode operation[13, 14]. In laser physics and applications, obtaining single-mode lasing is crucial since multi-mode operation will deteriorate the color purity and temporal stability by mode oscillation[23, 24]. Due to the typical large cavity length to provide sufficient gain for lasing action and the relatively broad gain bandwidth of traditional lasing materials, achieving single-mode lasing is still challenging[23, 24] and remains unaccomplished for $CsPbX_3$ IPNCs.

Vertical cavity surface emitting laser (VCSEL) is an important and much desired laser type which finds a broad range of applications like optical communication, high density optical storage, laser display, parallel optical computing and signal processing because of its ability to form 2-dimensional arrays, surface normal emission characteristics and high beam quality output ensuring easy coupling into an optical fibre[25, 26]. For any given gain materials, VCSELs represent the most tough laser configuration determined by the stringent criteria between gain and loss[6, 25]. As such, most surface normal devices were previously developed from complicated epitaxial growth of semiconductor heterostructures of many layers in which both bandgap alignment and lattice mismatch are big concerns[27-30]. The unavailability of independently adjusting the cavity and the active gain materials in an epitaxy based VCSEL makes material selection a constraint and the device cost ineffective. Thus, alternative fabrication of VCSELs with simplified processing is very appealing. Herein, we realized for the first time the high-performance VCSELs from solution-processed $CsPbX_3$ IPNCs. A clear evolution from spontaneous emission to lasing in the device upon optical pumping was manifested by the spectral narrowing, nonlinear increase of the PL intensity, drastic reduction of PL lifetime and remarkable decrease of output beam divergence. Both multi-mode and single-mode lasing operation have been achieved by tuning the cavity length. Thanks to the superior optical gain properties of the $CsPbBr_3$ IPNCs and the good match between the gain profile and the high reflectivity band of the distributed Bragg reflectors (DBRs), the lasing threshold of the IPNC-VCSELs is so low that quasi-continuous wave (q-CW) pumping is feasible. In contrast to traditional metal-chalcogenide CQD based lasers, where the thresholds for the green and blue are typically much higher than that of the red[6], these $CsPbX_3$ IPNC-VCSELs lase with comparable thresholds across the whole visible spectral range, which is promising in achieving single source-pumped full-color lasers. Our results highlight the resurging $CsPbX_3$ IPNCs in developing the challenging but practical lasers and shed light on the feasibility of independent adjustment of cavity and gain materials for the IPNC-VCSELs, which represent a great progress towards advanced laser sources based on the advantageous $CsPbX_3$ IPNCs.

Results

Modification of spontaneous emission from $CsPbBr_3$ IPNCs by microcavity effect. The $CsPbX_3$ IPNCs adopted here were synthesized following the method reported by Protesescu et al.[17] with slight adjustment[13]. The absorption and emission spectra of the $CsPbBr_3$ IPNCs are shown in Supplementary Fig. 1b, revealing the emission peak of ~504 nm with a narrow full-width at half maximum (FWHM) of ~21 nm. The corresponding transmission electron microscope (TEM) image (Supplementary Fig. 1a) displays the cubic shape with an edge length

of ~9 nm. To build the vertical microcavity, the commercially available dielectric DBRs consisted of 25 pairs of SiO_2/TiO_2 quarter-wave layers were employed as the high-reflective mirrors. Figure 1a displays the reflection spectrum of a DBR used here, which exhibits a stop-band from 430 nm to 570 nm, matching the PL spectrum of $CsPbBr_3$ IPNCs (see broadband reflection spectrum in Supplementary Fig. 2). The reflectivity was determined to be as high as 99.6% at ~500 nm. To sandwich the $CsPbBr_3$ IPNCs between two DBRs so as to form the prototypical VCSEL, the highly concentrated $CsPbBr_3$ IPNCs solution was spin-coated onto the top surface of a DBR, then, another DBR was brought upside-down in contact to the $CsPbBr_3$ IPNC film and finally fixed with glue. The schematic diagram (Fig. 1b), photograph (Supplementary Fig. 3) and the corresponding reflection spectrum ((Supplementary Fig. 2) of the final device are presented. Prior to the lasing investigation, the modification of spontaneous emission from $CsPbX_3$ IPNCs by the optical microcavity was interrogated, which could reflect the quality of the complete DBR resonator. Figure 1a shows the typical PL spectrum from the $CsPbBr_3$ IPNCs inserted within the cavity collected at 0° with respect to the surface normal (see Methods for details). In contrast to the PL spectrum from $CsPbX_3$ IPNCs spin-coated on a single DBR substrate, the PL within the cavity manifests multiple interference peaks, visualizing the presence of Fabry-Perot cavity effect. It is worth to note that the spiked emission is not laser but spontaneous emission modified by interference effect, which is further demonstrated by the following lifetime measurements (Fig. 2c). The resonant peaks can be assigned to mode numbers indexed as 29-33 based on the equation[31]: $m\lambda = 2nL$, where m is the mode number, λ is the emission wavelength, n is the refractive index of the $CsPbX_3$ IPNC film, L is the effective cavity length. L is estimated to be 4 μm assuming n=2[13]. By changing the thickness of the $CsPbBr_3$ IPNC film, the optical modes of the cavity and thus the PL spectrum can be tuned as exemplified in Supplementary Fig. 4. The slight red-shift of the envelop of the emission comb relative to the free-space emission spectrum can be attributed to the reabsorption effect due to the multipass of the radiation inside the cavity[24]. Furthermore, the spatial distribution of the radiation and the angle (θ) dependent PL spectrum from the device were examined by angle-resolved PL measurement (see Methods for details). It is found that the optical mode wavelengths gradually shift to blue as the detection angle increases (Fig. 2a), which quantitatively follows the equation: $m\lambda = 2nL\sqrt{n^2 - sin^2\theta}$ (Supplementary Fig. 5). Such behavior states nothing but that the radiation propagation angle inside the cavity and the detection angle are correlated by Snell's law (see detailed deviations in Supporting Information)[1, 31], further confirming that the discrete peaks originate from the Fabry-Perot interference. Notably, the radiation from the microcavity is much narrowed in space with respect to that from free-space $CsPbBr_3$ IPNCs (Fig. 2b), indicating that

spatially confined emission is obtained by the microcavity effect, which may shed light on developing $CsPbX_3$ IPNC-based light emitting diodes with directional radiation. Finally, the carrier dynamics of $CsPbBr_3$ IPNCs within/without microcavity was inspected by a streak camera system (Fig. 2c) (see the corresponding spectrograms in Supplementary Fig. 6). It is found that the PL decay curve within microcavity is almost identical to that in free space. A reduction of PL lifetime due to Purcell effect is not observed which can be attributed to the long cavity length and that the cavity mode only confined in one dimension[32].

Vertical cavity surface emitting lasers from $CsPbBr_3$ IPNCs. The stimulated emission from the close-packed thin film of the $CsPbBr_3$ IPNCs was first studied by stripe pumping configuration[13, 33] to exam the optical gain. As increasing the pumping density, the development of stimulated emission revealed by a much narrowed emission peak (FWHM: ~6.5 nm) can readily occur from our sample with a threshold of ~18 μJ/cm^2 (Supplementary Fig. 7). Such a low-threshold optical gain from $CsPbBr_3$ IPNCs in combination with the favorable coupling between the emission and the cavity modes motivates us to pursue $CsPbBr_3$ IPNC-based VCESLs. In doing so, the pump laser beam (400 nm, 100 fs) was focused by a circular lens (focus length: 5 cm) onto the device vertically, and the PL signal was collected from the surface normal of the cavity. A 30% reflection by the DBR for pump wavelength was extracted and counted in determining the final pump intensity. Figure 3a displays the evolution of PL spectra from the device as a function of pump intensity. Under relatively low pump intensities (< 11 μJ/cm^2), the PL spectra are dictated by spontaneous emission shaped by the cavity mode. With the increase of pump intensity, one of the discrete peaks with wavelength close to the stimulated emission spectra grows much faster than the others, which is accompanied by dramatic narrowing of the line-width down to ~0.6 nm. Figures 3b and c depict the change of PL intensity and the FWHM of the peaks corresponding to mode numbers from 29 to 33, respectively. The abrupt increase of the PL intensity and sudden decrease of the line-width of a particular peak indicate the achievement of lasing action[1, 34, 35]. The lasing threshold (P_{th}) is derived to be as low as 11 μJ/cm^2, which is much lower than that of the CdSe/CdZnS CQDs (65 μJ/cm^2), under similar conditions[6]. Importantly, due to the much larger free spectral range (*FSR*) of ~16 nm determined by the short cavity length than the stimulated emission line-width (6.5 nm), single-mode lasing operation was achieved. It should be noted that although the lasing peak locates at the blue side of the emission comb, it is actually on the red side of the spontaneous emission maximum of $CsPbBr_3$ IPNCs (Supplementary Fig. 8), in agreement with that the optical transition of the laser originates from the biexciton recombination[13, 36, 37].

To further verify the development of lasing, the PL dynamics as a function of pump intensity was investigated. Under pump intensity (0.1 P_{th}) of much lower than the threshold, the PL decay resembles the spontaneous emission trace. With the increase of pump intensity (0.8 P_{th}) approaching the threshold, a much faster decay channel, corresponding to the Auger recombination, appears. As the pump intensity (1.3 P_{th}) surpasses the threshold, the PL decay suddenly collapses to <50 ps, limited by the temporal resolution of the streak camera system, indicating the onset of lasing action[38].

Coherence and directionality are two basic features of a laser but are rarely examined in CQDs based lasers. Herein the directionality of the output radiation above and below the threshold is assessed by a CCD camera located 15 mm away from the laser device (inset in Fig. 3a) as well as angle-resolved PL measurement (Supplementary Fig. 9). We can see that when the pump intensity (1.3 P_{th}) exceeds the threshold, the divergence of the output signal remarkably decreases from 15º for spontaneous emission below P_{th} to 3.6º, thus a directional emission was obtained in our IPNC-VCSEL. Moreover, a clear interference pattern (Supplementary Fig. 10a) can be observed by using the conventional Michelson interference experiment[39, 40]. From the plot of the visibility ($V = \frac{I_{max}-I_{min}}{I_{max}+I_{min}}$, where I_{max} and I_{min} represent the intensities at the fringe maxima and minimum) as a function of detuning time or optical path difference[39, 40], the coherence time (τ) of ~1 ps can be derived (Supplementary Fig. 10c).

Finally, we test the stability of the device by monitoring the lasing peak intensity versus time at pump intensity of 1.5 P_{th} (pulse-width: 100 fs; repetition rate: 1KHz) (Supplementary Fig. 11). Thanks to the robustness of the $CsPbBr_3$ IPNCs, the output signal can maintain 80% of its initial value for more than one hour, which far excels the CdSe/CdZnS CQD-lasers[6].

Inspired by the excellent laser performance under femtosecond laser pump, it is highly promising to explore our IPNC-VCSEL pumped in the q-CW regime by a compact nanosecond laser[7, 41], which would be more practical and cost-effective. A ns laser pump is called the q-CW just because the pump duration is much longer than that of the effective gain (~35 ps)[42]. Figure 4a shows the pump intensity dependent PL spectra pumped by a Q-switched nanosecond laser (pulse-width: 5 ns; repetition rate: 20 Hz; wavelength: 400 nm). The onset of lasing action is unambiguously evidenced by the spectral narrowing and nonlinear increase of the PL intensity with respect to the pump intensity (inset in Fig. 4a) with a low threshold of 900 μJ/cm^2. To the best of our knowledge, this is the first demonstration of CQD-VCSEL operating in q-CW regime, which represents a significant step towards continuous wave and electrical pumping. The lasing

stability under nanosecond pumping is also examined (Supplementary Fig. 11). It is found that the lasing can last over one hour with losing only 50% of initial peak intensity. The faster decrease of the lasing intensity compared to that under femtosecond pump suggests the more serious thermal issue for long pump pulse duration[36]. So the effective thermal management (heat roll-off) shall be one of the major issues to address for future work toward stable CW operation[36, 43].

Furthermore, we demonstrate that multi-mode lasing operation can be produced in our IPNC-VCSELs via tuning the *FSR* to be smaller than the stimulated emission bandwidth which is enabled by increasing the effective cavity length (*L*) or film thickness of $CsPbBr_3$ IPNCs. Figure 4b illustrates the typical double mode lasing from the IPNC-VCSEL with *FSR* of ~6.2 nm and *L* of ~10.3 μm. Due to the longer cavity path and thus the lager round-trip gain, the lasing threshold further reduces to ~9.0 $\mu J/cm^2$ (inset in Fig. 4b).

Full-color VCSELs from $CsPbX_3$ IPNCs with comparable thresholds. For traditional metal-chalcogenide CQDs, the lasing wavelength is generally tuned by changing the dot size because of the band gap limit[2, 6]. For example, smaller dot size is necessitated to obtain green and blue lasers than that for red ones[6]. However, the optical loss including nonradiative AR and carrier trapping becomes more serious and the absorption cross-section reduces as the dot decreases, making the CQDs lase in short visible region challenging[2, 8]. Despite that lasing has been demonstrated from CQDs across the full visible range[6], the pump thresholds differ dramatically for red, green and blue colors, which hinders the realization of integrated full-color lasers with single pumping source[44]. In contrast, the emission color of $CsPbX_3$ IPNCs can be facilely tailored by composition control[17, 18]. By inserting the blue-emitting $CsPb(Br/Cl)_3$ IPNCs and red-emitting $CsPb(I/Br)_3$ IPNCs into the DBR resonators (for the red-emitting $CsPb(I/Br)_3$ IPNC-VCSEL, the DBR with stop-band centered at 590 nm was employed (Supplementary Fig. 12)), we successfully achieved IPNC-VCSELs across the full visible region (Fig. 5) (see full-range spectra in Supplementary Fig. 13 and Supplementary Fig. 14 for blue and red VCSELs, respectively). Notably, the lasing thresholds for the red (19.0 $\mu J/cm^2$) and blue (25.5 $\mu J/cm^2$) are comparable to that of the green, which indicates our $CsPbX_3$ IPNC-VECSELs may hold great promise for developing the single source-pumped full-color visible and white lasers.

Discussion

We for the first time realized the tough yet practically desirable VCSELs based on the emerging solution-processable $CsPbX_3$ IPNCs. The $CsPbX_3$ IPNC-VCSELs operate at a very low threshold,

so that the q-CW pumping is made feasible. Such a low lasing threshold can be mainly attributed to the large absorption cross-section of the $CsPbX_3$ IPNCs, high PL quantum yield, relatively low Auger loss and the good match between the gain profile and the stop-band of the DBRs[13, 14]. Especially, the absorption cross-section of the $CsPbX_3$ IPNCs was disclosed to be orders of magnitude higher than those of the metal-chalcogenide CQDs[13, 14, 42], which allows for the generation of excitons with denser concentration under the same pump density. Therefore, even though the $CsPbX_3$ IPNC-VCSELs stem from the biexciton recombination[13, 37], the pump thresholds for lasing still remain several times lower than that of the CdSe/CdZnS CQDs under similar conditions which was claimed to lase in single exciton regime[6]. Another advantage of the $CsPbBr_3$ IPNCs may be its cubic crystal shape. In general, dense packing of the nanocrystals in the ensemble film is essential for high effective gain and thus a low lasing threshold. In this regard, the cubic shape of $CsPbBr_3$ IPNCs is advantageous over the spherical ones of II-VI group metal-chalcogenide CQDs. The directionality and coherence from the laser device was clearly revealed. Taking advantage of the short cavity length and the narrow gain spectrum (~6.5 nm), single-mode lasing was achieved, attractive for various application fields. Noticeably, it is facile to independently choose the cavity characteristics and $CsPbX_3$ IPNCs for optimal match so that red, green and blue VCSELs can be realized with comparable pump thresholds, which is extremely difficult for epitaxial semiconductors and traditional metal-chalcogenide CQDs. We envisage that further optimization of the $CsPbX_3$ IPNCs, such as engineering the core/alloyed-shell heterostructure to mitigate the Auger and trapping loss[45], as well as adoption of proper thermal management in the device[36] could further reduce the lasing threshold and may eventually enable the continuous wave operation in the future.

Methods

Synthesis of $CsPbX_3$ IPNCs. Cs_2CO_3 (0.8 g), OA (oleic acid, 2.5 mL) and of ODE (octadecene, 30 mL) were mixed and kept in an argon atmosphere. The mixture was heated up to 130 ^oC for one hour. After that, the mixture was further heated up to 150 ^oC for reaction and lasted for 0.5 hour. Then, the solution was cooled down to room temperature. On the other side, 10 mL ODE, 1 mL OA and 0.36 mmol of PbX_2 (X=Cl, Br and I) were put together and kept in an argon atmosphere for one hour at temperature of 130 ^oC. Then, the solution was further heated up to 160 ^oC for reaction for 10 minutes. Finally, the Cs-precursor (1 mL) was quickly added into the

solution and cooled down by ice. More information about the synthesis of $CsPbX_3$ IPNCs can be found in reference 13.

Optical characterization. To investigate the modification of spontaneous emission from $CsPbX_3$ IPNCs by microcavity effect, the same femtosecond laser source (excitation wavelength: 400 nm, pulse-width: 100 fs, repetition rate: 1000 Hz) was employed as that used in the following lasing studies to maintain consistency. The excitation intensity was kept very low (0.5 $\mu J/cm^2$), far less than the threshold. We also have tried the continuous wave He-Cd laser as the excitation source, where similar spiked emission was observed, further confirming the spiked emission is not laser. The angle dependent PL signal was recorded as a function of detection direction by a home-built fiber-optics system. In particular, the collection fiber with diameter of 200 μm was attached to a 50 mm diameter rotating stage with the sample mounted at its center. The distance between the fiber and the sample is set as 15 mm. The other side of the fiber was coupled to a 320 mm monochromator combined with a charge coupled device detector. For the lasing investigation, the laser beam with wavelength of 400 nm generated by second harmonic generation from the seed with wavelength of 800 nm was focused by a circular lens (focus length: 5 cm) onto the VCSEL vertically, and the spot diameter on the sample was ~90 μm.The output signal was collected from the other side of the VCSEL by the above-mentioned fiber-optics system.

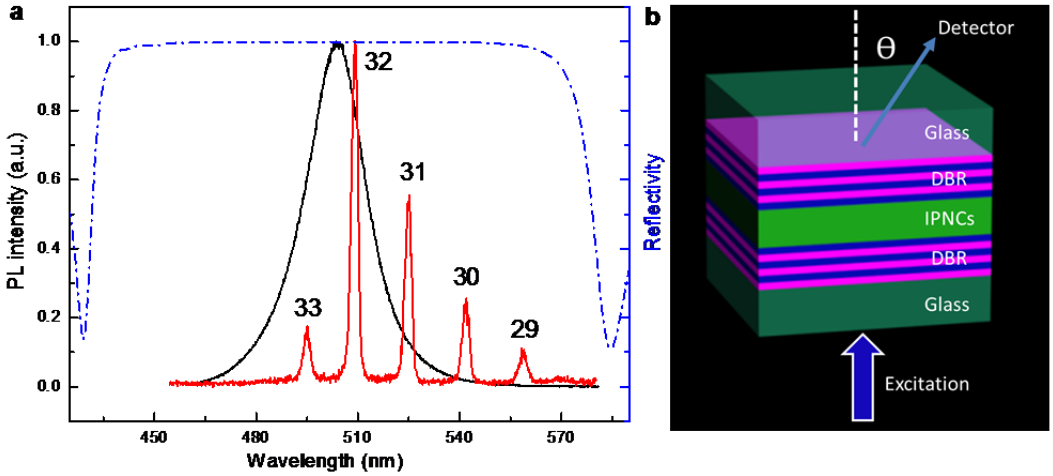

Figure 1| Modification of spontaneous emission from $CsPbBr_3$ IPNCs by presence of microcavity. (**a**) PL spectra from $CsPbBr_3$ IPNCs within (red line)/without (black line) microcavity under low excitation intensity of 0.5 μJ/cm^2. The blue dashed line represents the reflectivity of the adopted DBR. (**b**) Schematic configuration of the $CsPbBr_3$ IPNC-VCSEL.

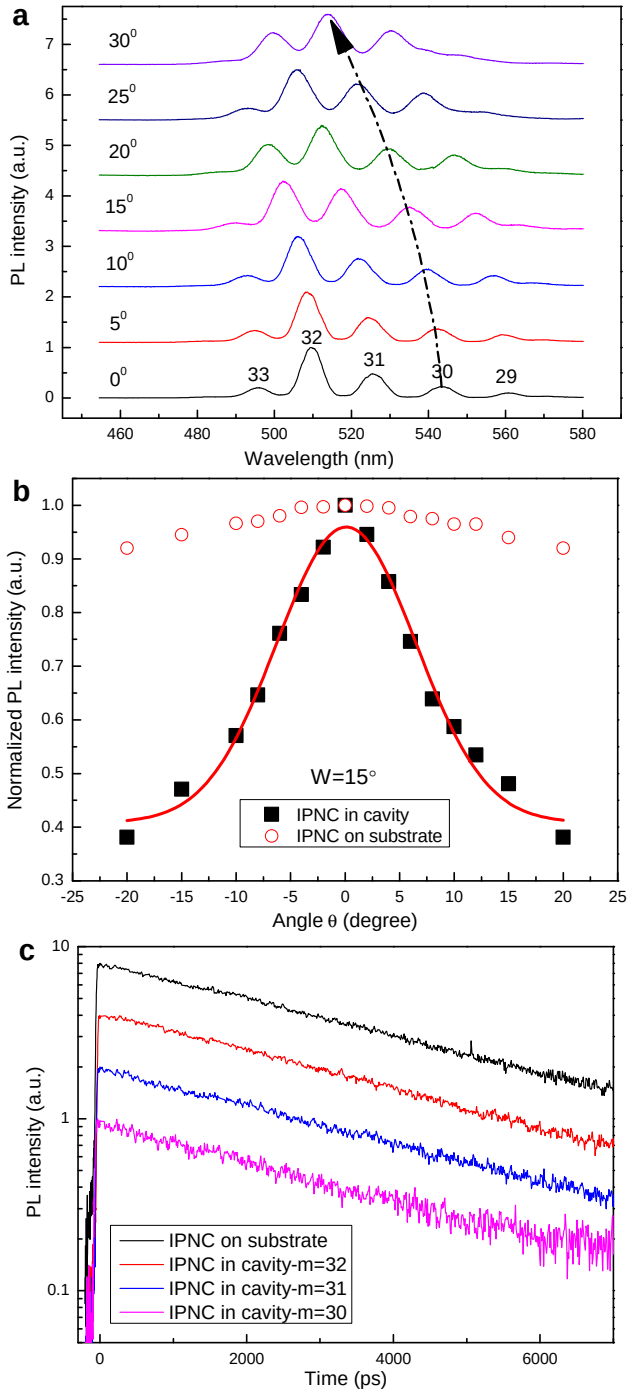

Figure 2| Angle-resolved PL from $CsPbBr_3$ IPNCs within microcavity and PL dynamics. (**a**) Detection angle dependent PL spectra from the $CsPbBr_3$ IPNCs within microcavity. (**b**) Spatial distribution of the irradiation from $CsPbBr_3$ IPNCs within/without microcavity. The PL signal greatly narrows with the presence of microcavity. The divergence is estimated to be 15º by Gaussian fitting (red line). (**c**) PL decay curves of $CsPbBr_3$ IPNCs within microcavity (mode number from 30 to 32) and that without microcavity.

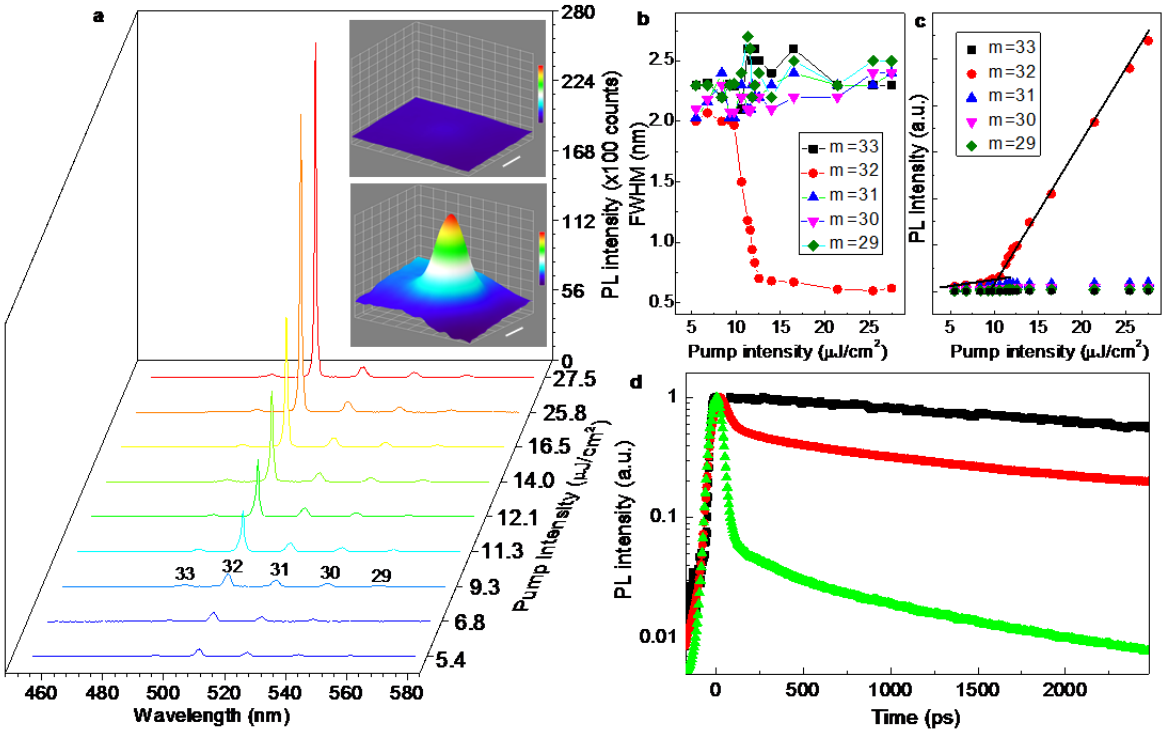

Figure 3| Vertical cavity surface emitting lasers from $CsPbBr_3$ IPNCs. (**a**) Pump intensity dependent PL spectra from the device. Insets shows the output beam profiles below (5.4 μJ/cm^2) (upper one) and above (25.8 μJ/cm^2) (bottom one) threshold. Scale bar is 1 mm. (**b**) Pump intensity dependent FWHM of the modes indexed from 29 to 33. (**c**) Pump intensity dependent PL intensity of the modes indexed from 29 to 33. (**d**) Pump intensity dependent PL decay curves of the device (0.1 P_{th} for the black curve, 0.8 P_{th} for the red curve and 1.3 P_{th} for the green curve)

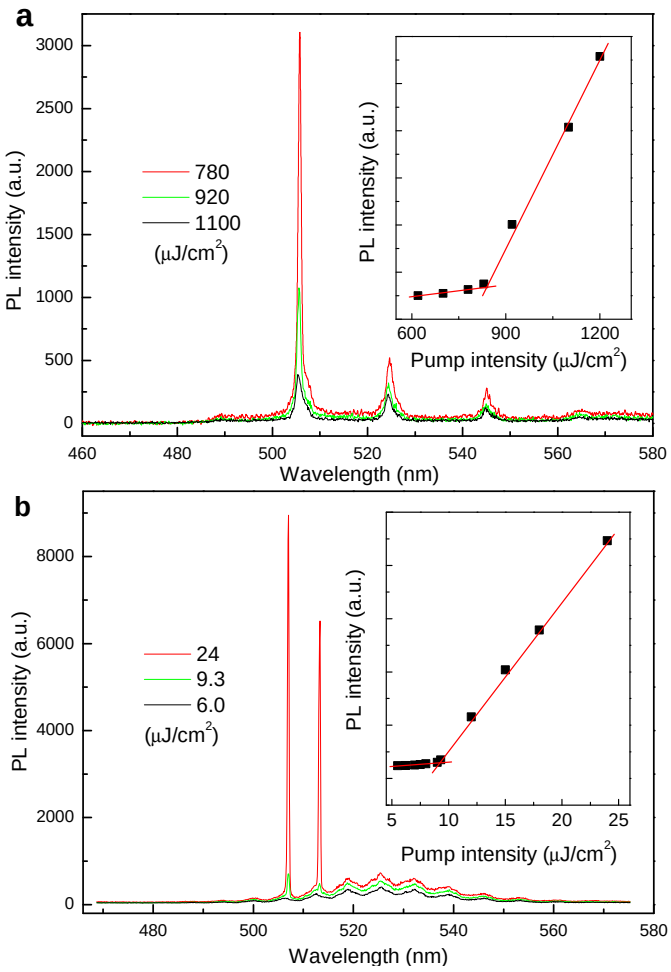

Figure 4| Lasing operation in quasi-continuous wave regime and multi-mode lasing. (**a**) Nanosecond laser pumped PL spectra as a function of pump intensity. The inset shows the integrated PL intensity over the sharp peak versus pump intensity. (**b**) Multi-mode lasing from the $CsPbBr_3$ IPNC-VCSEL. The inset shows the integrated PL intensity over the sharp peaks versus pump intensity.

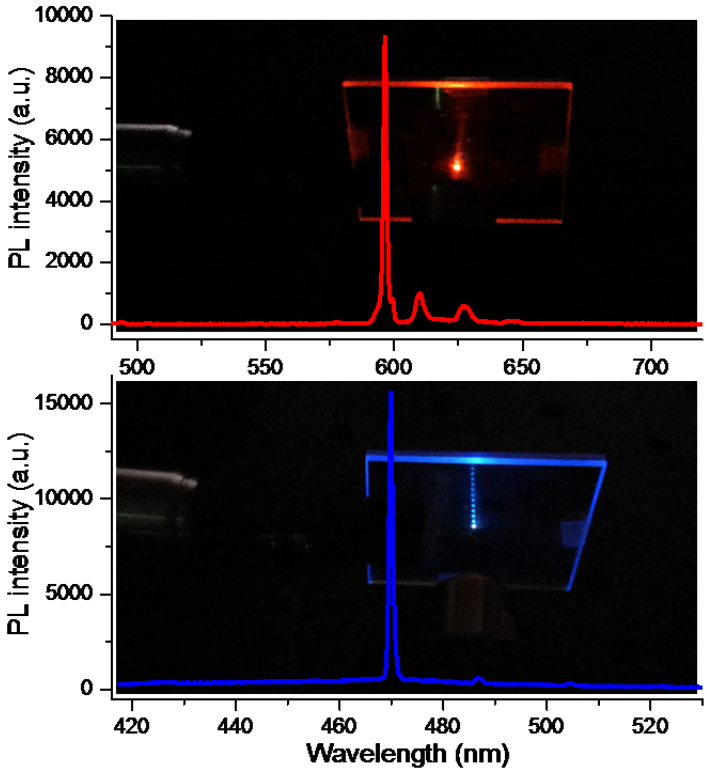

Figure 5| Red and blue vertical cavity surface emitting lasers from $CsPbX_3$ IPNCs. Red and blue lasing spectra of vertical cavity surface emitting lasers from $CsPb(I/Br)_3$ and $CsPb(Br/Cl)_3$ IPNCs under pump intensity of 30.5 and 38.2 $\mu J/cm^2$, respectively. The corresponding photograph of the device in operation is attached inside the plot.

1. Tessler, N., Denton, G.J. & Friend, R.H. Lasing from conjugated-polymer microcavities. *Nature* **382**, 695-697 (1996).
2. Klimov, V.I. et al. Optical gain and stimulated emission in nanocrystal quantum dots. *Science* **290**, 314-317 (2000).
3. Wang, Y. et al. Stimulated Emission and Lasing from CdSe/CdS/ZnS Core-Multi-Shell Quantum Dots by Simultaneous Three-Photon Absorption. *Adv. Mater.* **26**, 2954–2961 (2014).
4. Grim, J.Q. et al. Continuous-wave biexciton lasing at room temperature using solution-processed quantum wells. *Nature Nanotech.* **9**, 891-895 (2014).
5. Grivas, C. et al. Single-mode tunable laser emission in the single-exciton regime from colloidal nanocrystals. *Nature Commun.* **4**, 2376 (2013).
6. Dang, C. et al. Red, green and blue lasing enabled by single-exciton gain in colloidal quantum dot films. *Nature Nanotech.* **7**, 335-339 (2012).
7. Wang, Y. *et al*. Blue Liquid Lasers from Solution of CdZnS/ZnS Ternary Alloy Quantum Dots with Quasi-Continuous Pumping. *Adv. Mater.* **27**, 169-175 (2015).
8. Klimov, V.I., Mikhailovsky, A.A., McBranch, D.W., Leatherdale, C.A. & Bawendi, M.G. Quantization of multiparticle Auger rates in semiconductor quantum dots. *Science* **287**, 1011-1013 (2000).
9. Lee, M.M., Teuscher, J., Miyasaka, T., Murakami, T.N. & Snaith, H.J. Efficient Hybrid Solar Cells Based on Meso-Superstructured Organometal Halide Perovskites. *Science* **338**, 643-647 (2012).
10. Zhou, H. et al. Interface engineering of highly efficient perovskite solar cells. *Science* **345**, 542-546 (2014).
11. Deschler, F. et al. High Photoluminescence Efficiency and Optically Pumped Lasing in Solution-Processed Mixed Halide Perovskite Semiconductors. *J. Phys. Chem. Lett.* **5**, 1421-1426 (2014).
12. Zhu, H. et al. Lead halide perovskite nanowire lasers with low lasing thresholds and high quality factors. *Nature Mater.* **14**, 636-642 (2015).
13. Wang, Y. et al. All-Inorganic Colloidal Perovskite Quantum Dots: A New Class of Lasing Materials with Favorable Characteristics. *Adv. Mater.* **27**, 7101–7108 (2015).
14. Yakunin, S. et al. Low-threshold amplified spontaneous emission and lasing from colloidal nanocrystals of caesium lead halide perovskites. *Nature Commun.* **6** (2015).
15. Li, X. et al. CsPbX3 Quantum Dots for Lighting and Displays: Room-Temperature Synthesis, Photoluminescence Superiorities, Underlying Origins and White Light-Emitting Diodes. *Adv. Funct. Mate*r. **26**, 2435–2445 (2016).
16. Song, J. et al. Quantum Dot Light-Emitting Diodes Based on Inorganic Perovskite Cesium Lead Halides (CsPbX3). *Adv. Mater.***27**, 7162–7167 (2015).
17. Protesescu, L. et al. Nanocrystals of Cesium Lead Halide Perovskites (CsPbX3, X = Cl, Br, and I): Novel Optoelectronic Materials Showing Bright Emission with Wide Color Gamut. *Nano Lett.* (2015).
18. Akkerman, Q.A. et al. Tuning the Optical Properties of Cesium Lead Halide Perovskite Nanocrystals by Anion Exchange Reactions. *J. Am. Chem. Soc.***137**, 10276-10281 (2015).
19. Nedelcu, G. et al. Fast Anion-Exchange in Highly Luminescent Nanocrystals of Cesium Lead Halide Perovskites (CsPbX3, X = Cl, Br, I). *Nano Lett.* **15**, 5635-5640 (2015).
20. Swarnkar, A. et al. Colloidal CsPbBr3 Perovskite Nanocrystals: Luminescence beyond Traditional Quantum Dots. *Angew. Chem.*, n/a-n/a (2015).
21. Eaton, S.W. et al. Lasing in robust cesium lead halide perovskite nanowires. *Proc. Nat. Acad. Sci. U.S.A.* **113**, 1993-1998 (2016).
22. Eaton, S.W., Fu, A., Wong, A.B., Ning, C.-Z. & Yang, P. Semiconductor nanowire lasers. *Nature Reviews Materials* **1**, 16028 (2016).

23. Feng, L., Wong, Z.J., Ma, R.-M., Wang, Y. & Zhang, X. Single-mode laser by parity-time symmetry breaking. *Science* **346**, 972-975 (2014).
24. Xiao, Y. et al. Single-Nanowire Single-Mode Laser. *Nano Lett.* **11**, 1122-1126 (2011).
25. Sale, T.E. & Sale, T.E. Vertical cavity surface emitting lasers. (Research Studies Press, 1995).
26. Yoshikawa, T. et al. Complete polarization control of 8×8 vertical-cavity surface-emitting laser matrix arrays. *Appl. Phys. Lett.* **66**, 908-910 (1995).
27. Chen, R., Sun, H.D., Wang, T., Hui, K.N. & Choi, H.W. Optically pumped ultraviolet lasing from nitride nanopillars at room temperature. *Appl. Phys. Lett.* **96**, 241101 (2010).
28. Sun, H.D. et al. Low-loss 1.3-μm GaInNAs saturable Bragg reflector for high-power picosecond neodymium lasers. *Opt. Lett.* **27**, 2124-2126 (2002).
29. Calvez, S. et al. 1.3 μm GaInNAs optically-pumped vertical cavity semiconductor optical amplifier. *Electron. Lett* **39**, 100-102 (2003).
30. Chen, S. et al. Gain-switching dynamics in optically pumped single-mode InGaN vertical-cavity surface-emitting lasers. *Opt. Express* **22**, 4196-4201 (2014).
31. Marra, D.C., Aydil, E.S., Joo, S.-J., Yoon, E. & Srdanov, V.I. Angle-dependent photoluminescence spectra of hydrogenated amorphous silicon thin films. *Appl. Phys. Lett.* **77**, 3346-3348 (2000).
32. Qiao, H. et al. Optical properties of II-VI colloidal quantum dot doped porous silicon microcavities. *Appl. Phys. Lett.* **96**, 161106 (2010).
33. Wang, Y. et al. Nonlinear Absorption and Low-Threshold Multiphoton Pumped Stimulated Emission from All-Inorganic Perovskite Nanocrystals. *Nano Lett.* **16**, 448-453 (2016).
34. Samuel, I.D.W., Namdas, E.B. & Turnbull, G.A. How to recognize lasing. *Nature Photon.* **3**, 546-549 (2009).
35. Chen, Q., Kiraz, A. & Fan, X. Optofluidic FRET lasers using aqueous quantum dots as donors. *Lab on a Chip* **16**, 353-359 (2016).
36. Adachi, M.M. et al. Microsecond-sustained lasing from colloidal quantum dot solids. *Nature Commun.* **6** (2015).
37. Makarov, N.S. et al. Spectral and Dynamical Properties of Single Excitons, Biexcitons, and Trions in Cesium–Lead-Halide Perovskite Quantum Dots. *Nano Lett.* **16**, 2349-2362 (2016).
38. Liao, Q. et al. An Organic Microlaser Array Based on a Lateral Microcavity of a Single J-aggregation Microbelt. *Angew. Chem. Int. Ed.* **54**, 7037-7041 (2015).
39. Mhibik, O. et al. An ultra-narrow linewidth solution-processed organic laser. *Light Sci Appl* **5**, e16026 (2016).
40. Xu, D. et al. Polariton lasing in a ZnO microwire above 450 K. *Appl. Phys. Lett.* **104**, 082101 (2014).
41. Oron, D., Kazes, M. & Banin, U. Multiexcitons in type-II colloidal semiconductor quantum dots. *Phys. Rev. B* **75**, 035330 (2007).
42. Xu, Y. et al. Two-Photon-Pumped Perovskite Semiconductor Nanocrystal Lasers. *J. Am. Chem. Soc.* **138**, 3761-3768 (2016).
43. Kemp, A.J. et al. Thermal management in vertical-external-cavity surface-emitting lasers: finite-element analysis of a heatspreader approach. *IEEE J. Quantum Electron.* **41**, 148-155 (2005).
44. Fan, F., Turkdogan, S., Liu, Z., Shelhammer, D. & Ning, C.Z. A monolithic white laser. *Nature Nanotech.* **10**, 796-803 (2015).
45. Wang, Y. et al. Unraveling the ultralow threshold stimulated emission from CdZnS/ZnS quantum dot and enabling high-Q microlasers. *Laser Photonics Rev.* **9**, 507-516 (2015).

Acknowledgements

This research is supported by the Singapore National Research Foundation through the Competitive Research Programme (CRP) under Project No. NRFCRP6-2010-02, the Singapore Ministry of Education through the Academic Research Fund under Projects Tier 1- RG92/15 and MOE 2011-T3-1-005 (Tier 3), and National Basic Research Program of China (grant number 2014CB931700).

Author contribution

All authors contributed extensively to this work. Y.W. and V.N. conducted spectroscopic experiment and analysis. Y.W. and H.S. conceived and fabricated the VCSEL structure. X.L. and H.Z. synthesized the IPNC samples. H.S. and H.Z. supervised the project. Y.W., X.L., V.N., H.Z., and H.S. analyzed data and interpreted the results, and wrote the manuscript with input from all authors.